 CMES, vol.27, no.1, pp.49-62, 2008

Vibration and Control of Rotating Tapered Thin-Walled Composite Beam Using Macro Fiber Composite Actuator

Vadiraja D. N.[1] **and A. D. Sahasrabudhe**[2]

Abstract: Rotating beams are flexible structures, which are often idealized as cantilever beams. Structural modelling of rotating thin-walled composite beam with embedded MFC actuators and sensors using higher shear deformation theory (HSDT) is presented. A non-Cartesian deformation variable (which represents arc length stretch) is used along with two Cartesian deformation variables. The governing system of equations is derived from Hamilton's principle and solution is obtained by extended Galerkin's method. Optimal control problem is solved using LQG control algorithm. Vibration characteristics and optimal control for a box beam configuration are discussed in numerical examples. Gyroscopic coupling between lagging-extension motions is found to have significant effect and cannot be neglected. Effects of bending vibration suppression using MFC actuators and sensors are highlighted.

Keyword: HSDT, LQG, MFC, Thin-walled beams.

1 Introduction

Turbo machines, helicopter blades, tilt rotor aircrafts, robot manipulators, compressors, spinning space structures and henceforth can be modeled as rotating cantilever beams. The forces transmitted from the rotating cantilever beams are a source of vibration. This results in inefficient working of a system. The vibration control is necessary for safe and efficient working of these structures. It is well known that thin walled composite materials facilitate substantial reduction in weight or increase load carrying capacities, superior fatigue characteristics and facilitate structural tailoring.

Experimental and theoretical analysis of free vibration characteristics of the rotating composite box beams with elastic coupling using small deflection theory have studied by Ramesh and Inderjit (1992). A finite element formulation for thin walled composite beam with first order shear deformation that is free from shear locking is presented by Mitra; Gopalakrishnan and Bhat (2004a). This beam element is having super convergent property and which is used for wave propagation analysis. Further, Vinod, Gopalakrishnan and Ganguli (2006; 2007) presented spectral finite element of rotating isotropic Euler-Bernoulli beam. Higher order shear deformation theory (HSDT) was developed for thin walled composite beams by Suresh and Nagaraj (1996). The rotating thin walled composite beam was analyzed by Chandiramani; Librescu and Shete (2002). Song and Librescu (1997), and Chandiramani; Librescu and Shete (2002) have used geometrically non-linear modeling method for deriving coupled equations of motion including centrifugal stiffening and gyroscopic coupling. However, this approach leads to cumbersome formulation procedure and non inclusion of gyroscopic coupling in numerical analysis because linearization is possible only after discarding gyroscopic coupling. In order to overcome this, Kane; Ryan and Banerjee (1987) and Yoo; Rayn and Scott (1995) have used a new method for the rotating beams. This method was named as dynamic modeling method by Yoo and Shin (1998). Kane; Ryan and Banerjee (1987) have shown that centrifugal stiffening and gyroscopic coupling can be captured without considering large deformations. Dynamic modeling method employs a non-Cartesian deformation variable in addition to two Cartesian deformation variables and linear Cauchy strain measures. In

[1] Indian Institute of Technology, Guwahati, India.
[2] Indian Institute of Technology, Guwahati, India. On deputation, Director, College of Engineering Pune, India.

the above method, the hybrid set of deformation variables consist of arc length stretch, flapwise deformation and lagwise deformation. Yoo; Rayn and Scott (1995) showed that this transformation is equivalent to considering von Korman strain measures for the beam. Recently, Yoo; Lee and Shin (2005) have studied flapwise free vibration studies of composite cantilever beam using this method.

Lately, the vibration suppression using piezoelectric material has been a major research area. Sungsoo and Liviu (2000) studied optimal feedback control of shearable composite cantilever beam. Vibration control of thin walled beam using acceleration feedback is presented by Mitra; Gopalakrishnan and Bhat (2004b). Vasques and Rodrigues (2006) have investigated the performance of different control strategies in smart active piezoelectric beam. Narayanan and Balamurugan (2003) have presented the active vibration control performance of shear deformable piezolaminated beam, plate and shell using finite element method. The study of optimal vibration control of rotating composite beam with embedded piezoelectric sensors and actuators is reported by Chandiramani; Librescu; Saxena and Kumar (2004). Reddy (1999) developed shear deformation composite plate theory with integrated sensors and actuators. In all these works, monolithic piezoelectric materials are used which are brittle in nature. Recently, piezoelectric fibre based sensors and actuators are attracting attention of researchers. Different kinds of piezoelectric fibre composites developed in recent years are active fibre composites (AFC) developed by Bent; Hagood and Rodgers (1995), macro fibre composites (MFC) developed by Wilkie; Belvin and Park (1996) and piezoelectric fibre reinforced composite (PFRC) developed by Nilanjan and Ray (2004). MFC sensors and actuators are having numerous advantages over monolithic piezoelectric materials are discussed by Park and Kim (2005) in detail. Henry; Gyuhae and Daniel (2004) experimentally investigated the performance of MFC for sensing applications in inflated torus. Brockmann and Lammering (2006) formulated beam element for rotating thin walled composite beams and studied vibration characteristics. Choi; Park and Kim (2006; 2007) modelled first order shear deformation theory of rotating thin walled beams using MFC actuators and monolithic piezoelectric sensors. In their study, the negative velocity feedback control algorithm is used to suppress the vibration. Analysis of damping performance by placing sensors and actuators on inner, central and outer surface of the box beam has been carried out by Choi; Park and Kim (2006).

The purpose of the present study is to model the dynamic modelling method to thin-walled composite material with embedded MFC actuators and sensors. The coupled linear equations of motion describing axial, bending and rotational motions, including gyroscopic coupling and centrifugal stiffening are derived based on Hamilton's principle. Extended Galerkin's method is used to obtain an approximate solution. Linear Quadratic Gaussian (LQG) output feedback controller is used for optimal control with sensor current as output. Numerical solutions are illustrated for a box beam configuration.

2 2 Formulation

A composite beam of length L and hub radius R_o, rotating with constant angular velocity Ω is considered. The Cartesian inertial frame of reference (X, Y, Z) has its origin at the centre of the hub. The beam coordinate system (x, y, z) is located at offset R_o from the origin O. Further, (i, j, k) and (I, J, K) represent unit vectors in (x, y, z) and (X, Y, Z) coordinate systems respectively (Figs. 1(a) and 1(b)). In addition to above, a local coordinate system (s, n, z) associated with the beam is also considered which is shown in Fig. 1(b). Taper parameters in the beam are taken as $\eta = \frac{cr}{ct} = \frac{br}{bt}$, where, cr, ct, br and bt are the chord and breadth at root and tip of the beam respectively. Midline cross-section profile can be written as,

$$\begin{aligned} c(z) &= \frac{cr}{\eta}\left[1+\frac{(\eta-1)(L-z)}{L}\right]; \\ b(z) &= \frac{br}{\eta}\left[1+\frac{(\eta-1)(L-z)}{L}\right] \end{aligned} \tag{1}$$

Instead of w, a non-Cartesian variable $\hat{s}$ denot-

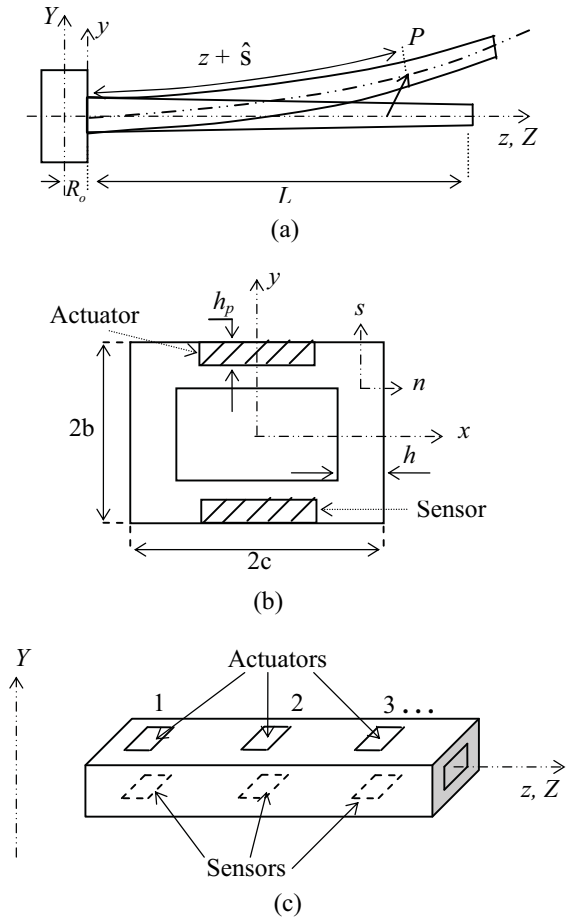

Figure 1: Beam configuration and coordinate system (a) beam geometry (b) beam cross-section (c) sensors and actuators distribution

ing axial stretch is used in the present study. u, v and $\hat{s}$ represent displacements along (x, y, z) axes respectively and θ_x, θ_y, ϕ represent rotations about (x, y, z) axes respectively. The displacements $\hat{s}$ and w are related by [Yoo; Rayn and Scott (1995)],

$$\hat{s} = w + \frac{1}{2}\int_0^z \left[\left(\frac{\partial u}{\partial \sigma}\right)^2 + \left(\frac{\partial v}{\partial \sigma}\right)^2\right] \mathrm{d}\sigma \tag{2}$$

The embedded MFC actuators and sensors are distributed over the top and bottom surface of the beam, respectively as shown in Figs. 1(b) and 1(c). Linear displacements u, v and w representing lag, flap and extensional motion respectively, are obtained for shearable beam as in [Chandiramani; Librescu and Shete (2002)],

$$u = u_o + z\phi \tag{3}$$

$$v = v_o - x\phi \tag{4}$$

$$\begin{aligned} w =& w_o + [\overline{y} + nm]\,\theta_x - [\overline{x} + nl]\,\theta_y - [F_w + na]\,\phi' \\ &+ \frac{4n^3}{3h^2}\left[l\left(\theta_y - u_o'\right) - m\left(\theta_x + v_o'\right)\right] \end{aligned} \tag{5}$$

From Eqs. 2 and 5, the axial displacement component in arc length stretch coordinate system is

$$\begin{aligned} \hat{s} =& w_o + [\overline{y} + nm]\,\theta_x - [\overline{x} + nl]\,\theta_y - [F_w + na]\,\phi' \\ &+ \frac{4n^3}{3h^2}\left[l\left(\theta_y - u_o'\right) - m\left(\theta_x + v_o'\right)\right] \\ &+ \frac{1}{2}\int_0^z \left[\left(\frac{\partial u}{\partial \sigma}\right)^2 + \left(\frac{\partial v}{\partial \sigma}\right)^2\right] \mathrm{d}\sigma \end{aligned} \tag{6}$$

where $l = \frac{\mathrm{d}\overline{y}}{\mathrm{d}s}$; $m = -\frac{\mathrm{d}\overline{x}}{\mathrm{d}s}$; $a = m\overline{x} - l\overline{y}$. F_w and na represents primary and secondary warping functions respectively.

2.1 Piezoelectric constitutive equation

Strain in a piezoelectric material produces electrical charge, which is referred as direct piezoelectric effect. Conversely induced electric field in a piezoelectric material results in a strain, which is known as converse piezoelectric effect. The standard linear piezoelectric constitutive relation representing the direct and converse effect can be written as,

$$\begin{aligned} D &= e\varepsilon + \in E \\ \sigma &= C\varepsilon - e^{\mathrm{T}}E \end{aligned} \tag{7}$$

where D, e, $\in$, E, ε, σ and C are electric displacement, piezoelectric constant, permittivity coefficient, electric field, strain, stress and elastic constant respectively. Assuming the piezoelectric fiber composite to be transversely isotropic in fibre direction, converse piezoelectric effect can be written as [Choi; Park and Kim (2006; 2007)],

$$\begin{Bmatrix} \sigma_{11}^p \\ \sigma_{22}^p \\ \sigma_{33}^p \\ \sigma_{23}^p \\ \sigma_{13}^p \\ \sigma_{12}^p \end{Bmatrix} = \begin{bmatrix} C_{11} & C_{12} & C_{13} & 0 & 0 & 0 \\ C_{12} & C_{11} & C_{13} & 0 & 0 & 0 \\ C_{13} & C_{13} & C_{33} & 0 & 0 & 0 \\ 0 & 0 & 0 & C_{44} & 0 & 0 \\ 0 & 0 & 0 & 0 & C_{44} & 0 \\ 0 & 0 & 0 & 0 & 0 & \frac{C_{11}-C_{12}}{2} \end{bmatrix} \begin{Bmatrix} \varepsilon_{11}^p \\ \varepsilon_{22}^p \\ \varepsilon_{33}^p \\ \gamma_{23}^p \\ \gamma_{13}^p \\ \gamma_{12}^p \end{Bmatrix} - \begin{Bmatrix} e_{11} \\ e_{12} \\ e_{13} \\ 0 \\ 0 \\ 0 \end{Bmatrix} E_1 \quad (8)$$

Assuming that the through thickness stress is negligible and piezoelectric fiber is aligned at θ_p from the positive s-axis, the transformed reduced constitutive equation for piezoelectric material can be written as

$$\begin{Bmatrix} \sigma_{ss}^p \\ \sigma_{zz}^p \\ \tau_{sz}^p \end{Bmatrix} = \begin{bmatrix} \overline{Q}_{11}^p & \overline{Q}_{12}^p & \overline{Q}_{16}^p \\ \overline{Q}_{12}^p & \overline{Q}_{22}^p & \overline{Q}_{26}^p \\ \overline{Q}_{16}^p & \overline{Q}_{26}^p & \overline{Q}_{66}^p \end{bmatrix} \begin{Bmatrix} \varepsilon_{ss}^p \\ \varepsilon_{zz}^p \\ \gamma_{sz}^p \end{Bmatrix} - \begin{Bmatrix} \overline{e}_{ss} \\ \overline{e}_{zz} \\ \overline{e}_{sz} \end{Bmatrix} E_1$$
$$\begin{Bmatrix} \tau_{nz}^p \\ \tau_{sn}^p \end{Bmatrix} = \begin{bmatrix} \overline{Q}_{44}^p & 0 \\ 0 & \overline{Q}_{44}^p \end{bmatrix} \begin{Bmatrix} \gamma_{nz}^p \\ \gamma_{sn}^p \end{Bmatrix} \quad (9)$$

Piezoelectric constant matrix $\overline{e}$ can be written in the form of piezoelectric strain constant matrix d and elastic constants $\overline{Q}_{ij}$ as [Lam; Peng; Liu and Reddy (1997)]

$$[\overline{e}] = [d]\left[\overline{Q}_{ij}^p\right] \quad (10)$$

2.2 Passive composite constitutive equation

Transformed reduced stiffness matrix for composite passive host structure for the k^{th} layer is written as [Chandiramani; Librescu and Shete (2002)]

$$\begin{Bmatrix} \sigma_{ss}^h \\ \sigma_{zz}^h \\ \tau_{sz}^h \end{Bmatrix}_k = \begin{bmatrix} \overline{Q}_{11}^h & \overline{Q}_{12}^h & \overline{Q}_{16}^h \\ \overline{Q}_{12}^h & \overline{Q}_{22}^h & \overline{Q}_{26}^h \\ \overline{Q}_{16}^h & \overline{Q}_{26}^h & \overline{Q}_{66}^h \end{bmatrix}_k \begin{Bmatrix} \varepsilon_{ss}^h \\ \varepsilon_{zz}^h \\ \gamma_{sz}^h \end{Bmatrix}_k \quad (11)$$
$$\begin{Bmatrix} \tau_{nz}^h \\ \tau_{sn}^h \end{Bmatrix}_k = \begin{bmatrix} \overline{Q}_{44}^h & \overline{Q}_{45}^h \\ \overline{Q}_{45}^h & \overline{Q}_{55}^h \end{bmatrix}_k \begin{Bmatrix} \gamma_{nz}^h \\ \gamma_{sn}^h \end{Bmatrix}_k$$

2.3 Combined composite host and piezoelectric constitutive equation

From Eqs. 9 and 11 combined constitutive equation for host and piezoelectric material can be written as,

$$\begin{Bmatrix} \sigma_{ss} \\ \sigma_{zz} \\ \tau_{sz} \end{Bmatrix} = \begin{bmatrix} \overline{Q}_{11} & \overline{Q}_{12} & \overline{Q}_{16} \\ \overline{Q}_{12} & \overline{Q}_{22} & \overline{Q}_{26} \\ \overline{Q}_{16} & \overline{Q}_{26} & \overline{Q}_{66} \end{bmatrix} \begin{Bmatrix} \varepsilon_{ss} \\ \varepsilon_{zz} \\ \gamma_{sz} \end{Bmatrix} - \begin{Bmatrix} \overline{e}_{ss} \\ \overline{e}_{zz} \\ \overline{e}_{sz} \end{Bmatrix} E_1$$
$$\begin{Bmatrix} \tau_{nz} \\ \tau_{sn} \end{Bmatrix} = \begin{bmatrix} \overline{Q}_{44} & \overline{Q}_{45} \\ \overline{Q}_{45} & \overline{Q}_{55} \end{bmatrix} \begin{Bmatrix} \gamma_{nz} \\ \gamma_{sz} \end{Bmatrix} \quad (12)$$

where $\overline{Q}_{ij} = \overline{Q}_{ij}^h + \left(\overline{Q}_{ij}^p - \overline{Q}_{ij}^h\right) H(s,z,n)$. $H(s,z,n)$ is the Heaviside function and takes value 1 when integrating over piezoelectric material and 0 for host structure.

2.4 Equation of motion

The Hamilton's variational equation is written as,

$$\int_{t_1}^{t_2} [\delta T - \delta V + \delta W] \mathrm{d}t = 0 \quad (13)$$

where

$$\delta V = \int_\tau \sigma_{ij} \delta \varepsilon_{ij} \mathrm{d}\tau \quad (14)$$

$$\delta T = -\int_\tau \rho(\ddot{\mathbf{R}}_\mathbf{i} \cdot \delta \mathbf{R}_\mathbf{i}) \mathrm{d}\tau \quad (15)$$

The position vector relative to the fixed origin $O$of a point on the deformed beam is obtained as, $\mathbf{R} = R_o\mathbf{k} + x\mathbf{i} + y\mathbf{j} + z\mathbf{k} + u\mathbf{i} + v\mathbf{j} + w\mathbf{k}$. Differentiating twice with respect to time, the acceleration of point P can be written as,

$$\ddot{\mathbf{R}} = \left(\ddot{u} + 2\Omega\dot{w} - \Omega^2(x+u)\right)\mathbf{I} + \ddot{v}\mathbf{J} + \left(\ddot{w} - 2\Omega\dot{u} - \Omega^2(R_o + z + w)\right)\mathbf{K} \quad (16)$$

Variational potential energy can be derived by substituting Eqs. 3, 4, 6, 12 and strain displacement relations (Appendix A) in Eq. 14. Variational kinetic energy can be derived by substituting Eqs. 3, 4, 6 and 16 in Eq. 15. Finally, substituting obtained kinetic and potential energies in Hamilton's principle, one can write equations of motion,

$$\begin{aligned}\delta u_o :&\tilde{a}_4(\theta_x'' + v_o''') - \tilde{a}_5\theta_y''' + \tilde{a}_6 u_o^{IV} - (a_{43}+\tilde{a}_2)\theta_x'' \\ &+ (a_{44}+\tilde{a}_1)(\theta_y' - u_o'') - \tilde{a}_3 v_o''' \\ &+ b_1(\ddot{u}_o - 2\Omega\dot{w}_o - \Omega^2 u_o) + (\tilde{M}_6 - \tilde{M}_4)\tilde{I}_{mm}\ddot{\theta}_y' \\ &+ \tilde{M}_6\tilde{I}_{mm}\ddot{u}_o'' - \Omega^2[(\tilde{M}_6 - \tilde{M}_4)\tilde{I}_{mm}\theta_y' \\ &+ \tilde{M}_6\tilde{I}_{mm}u_o'' - R_z b_1 u_o''] - (E_1\tilde{a}_3^p)' = 0\end{aligned} \tag{17}$$

$$\begin{aligned}\delta v_o :&\tilde{a}_3(-\theta_y'' + u_o''') + \tilde{a}_9\theta_x''' + \tilde{a}_{10}v_o^{IV} \\ &+ (a_{52}+\tilde{a}_8)\theta_y'' - \tilde{a}_4 u_o''' \\ &- (a_{55}+\tilde{a}_7)(\theta_x' + v_o'') + b_1\ddot{v}_o \\ &- (\tilde{M}_6 - \tilde{M}_4)\tilde{I}_\mu\ddot{\theta}_x' - \tilde{M}_6\tilde{I}_\mu\ddot{v}_o'' + 2\Omega\tilde{M}_4\tilde{I}_\mu\dot{\phi}' \\ &- \Omega^2[-(\tilde{M}_6 - \tilde{M}_4)\tilde{I}_\mu\theta_x' - \tilde{M}_6\tilde{I}_\mu v_o'' - R_z b_1 v_o''] \\ &+ (E_1\tilde{a}_4^p)'' = 0\end{aligned} \tag{18}$$

$$\begin{aligned}\delta w_o :&-a_{11}w_o'' - a_{17}\phi'' \\ &+ b_1\left(\ddot{w}_o - 2\Omega\dot{u}_o - \Omega^2(R_o + z + w_o)\right) \\ &- (E_1\tilde{a}_1^p)' = 0\end{aligned} \tag{19}$$

$$\begin{aligned}\delta\theta_x :&(a_{55}+\tilde{a}_7)(\theta_x + v_o') - (a_{52}+\tilde{a}_8)\theta_y' + \tilde{a}_4 u_o'' \\ &- (a_{33}+\tilde{a}_2)\theta_x'' + (a_{43}+\tilde{a}_2)(-\theta_y' + u_o'') \\ &- \tilde{a}_9 v_o''' + 2\Omega(I_{xx} - \tilde{M}_4\tilde{I}_\mu)\dot{\phi} + I_{xx}\ddot{\theta}_x \\ &+ (\tilde{M}_6 - \tilde{M}_4)\tilde{I}_\mu(\ddot{\theta}_x + \ddot{v}_o') - \tilde{M}_4\tilde{I}_\mu\ddot{\theta}_x \\ &- \Omega^2[I_{xx}\theta_x + (\tilde{M}_6 - \tilde{M}_4)\tilde{I}_\mu(\theta_x + v_o') \\ &- \tilde{M}_4\tilde{I}_\mu\theta_x] - (E_1\tilde{a}_6^p)' = 0\end{aligned} \tag{20}$$

$$\begin{aligned}\delta\theta_y :&(a_{44}+\tilde{a}_1)(\theta_y - u_o') - (a_{43}+\tilde{a}_2)\theta_x' + \tilde{a}_3 v_o'' \\ &- (a_{22}+\tilde{a}_{11})\theta_y'' + (a_{52}+\tilde{a}_8)(\theta_x' + v_o'') \\ &+ \tilde{a}_5 u_o''' + (\tilde{M}_6 - \tilde{M}_4)\tilde{I}_{mm}(\ddot{\theta}_y - \ddot{u}_o') \\ &+ I_{yy}\ddot{\theta}_y - \tilde{M}_4\tilde{I}_{mm}\ddot{\theta}_y \\ &- \Omega^2[I_{yy}\ddot{\theta}_y + (\tilde{M}_6 - \tilde{M}_4)\tilde{I}_{mm}(\ddot{\theta}_y - \ddot{u}_o') \\ &- \tilde{M}_4\tilde{I}_{mm}\ddot{\theta}_y] + (E_1\tilde{a}_9^p) = 0\end{aligned} \tag{21}$$

$$\begin{aligned}\delta\phi :&-a_{77}\phi'' - a_{17}w_o'' + a_{66}\phi^{IV} + (I_{xx}+I_{yy})\ddot{\phi} \\ &- I_{ww}\ddot{\phi}'' + 2\Omega\left[(\tilde{M}_4\tilde{I}_\mu - I_{xx})\dot{\theta}_x + \tilde{M}_4\tilde{I}_\mu\dot{v}_o'\right] \\ &- \Omega^2[I_{xx}\phi - I_{ww}\phi'' - R_z b_1(I_{xx}+I_{yy})] \\ &- (E_1\tilde{a}_{10}^p)' = 0\end{aligned} \tag{22}$$

The forced boundary conditions are obtained as,

$$\begin{aligned}\delta u_o :&\tilde{a}_5\theta_y'' - \tilde{a}_4(\theta_x' + v_o'') - \tilde{a}_6 u_o''' \\ &- (a_{44}+\tilde{a}_1)(\theta_y - u_o') + \tilde{a}_3 v_o'' + (a_{43}+\tilde{a}_2)\theta_x' \\ &+ (\tilde{M}_6 - \tilde{M}_4)\tilde{I}_{mm}\ddot{\theta}_y + \tilde{M}_6\tilde{I}_{mm}\ddot{u}_o' \\ &+ \Omega^2[-(\tilde{M}_6 - \tilde{M}_4)\tilde{I}_{mm}\theta_y - \tilde{M}_6\tilde{I}_{mm}u_o' \\ &- R_z b_1 u_o'] + E_1\tilde{a}_3^p = 0\end{aligned} \tag{23}$$

$$\delta u_o' :\ \tilde{a}_4(\theta_x + v_o') - \tilde{a}_5\theta_y' + \tilde{a}_6 u_o'' = 0 \tag{24}$$

$$\begin{aligned}\delta v_o :&\tilde{a}_3(\theta_y' - u_o'') - \tilde{a}_9\theta_x'' - \tilde{a}_{10}v_o''' \\ &+ (a_{55}+\tilde{a}_7)(\theta_x + v_o') + \tilde{a}_4 u_o'' \\ &- (a_{52}+\tilde{a}_8)\theta_y' + (\tilde{M}_6 - \tilde{M}_4)\tilde{I}_\mu\ddot{\theta}_x + \tilde{M}_6\tilde{I}_\mu\ddot{v}_o' \\ &- \Omega^2[(\tilde{M}_6 - \tilde{M}_4)\tilde{I}_\mu\theta_x + \tilde{M}_6\tilde{I}_\mu v_o' - R_z b_1 v_o'] \\ &- E_1\tilde{a}_4^p = 0\end{aligned} \tag{25}$$

$$\delta v_o' :\ +\tilde{a}_3(-\theta_y + u_o') + \tilde{a}_9\theta_x' + \tilde{a}_{10}v_o'' = 0 \tag{26}$$

$$\delta w_o :\ a_{11}w_o' + a_{17}\phi' + E_1\tilde{a}_1^p = 0 \tag{27}$$

$$\begin{aligned}\delta\theta_x :&(a_{33}+\tilde{a}_{12})\theta_x' - (a_{43}+\tilde{a}_2)(\theta_y - u_o') \\ &+ \tilde{a}_9 v_o'' + E_1\tilde{a}_6^p = 0\end{aligned} \tag{28}$$

$$\begin{aligned}\delta\theta_y :&(a_{22}+\tilde{a}_{11})\theta_y' - (a_{52}+\tilde{a}_8)(\theta_x + v_o') \\ &- \tilde{a}_5 u_o'' = 0\end{aligned} \tag{29}$$

$$\begin{aligned}\delta\phi :&a_{77}\phi' + \tilde{a}_{17}w_o' - a_{66}\phi''' + I_{ww}\ddot{\phi}' \\ &+ \Omega^2(-I_{ww}\phi' + R_z b_1(I_{xx}+I_{yy})\phi'') \\ &+ E_1\tilde{a}_{10}^p = 0\end{aligned} \tag{30}$$

$$\delta\phi' :\ a_{66}\phi'' \tag{31}$$

where $R(z) = R_o(L-z) + 0.5(L^2 - z^2)$. Global stiffness quantities a_{ij}, $\tilde{a}_{ij}$ and inertia quantities for passive host structure are described by Song and Librescu (1997) and Chandiramani; Librescu

and Shete (2002) respectively. Global stiffness quantities $\tilde{a}^p_{ij}$ of piezoelectric material are described in Appendix B.

The underlined terms in Eqs. 17-18 and 22 are centrifugal stiffening terms. Song and Librescu (1997) captured centrifugal stiffening effect using geometrically nonlinear modelling method. In their approach, a set of nonlinear equations of motion are derived. Neglecting gyroscopic coupling and using suitable assumptions nonlinear extension equation of motion is decoupled and integrated to obtain axial force. This axial force is substituted in the equation of motion to obtain centrifugal stiffening effect.

However in the present method, a non-Cartesian deformation variable representing axial stretch, along with two Cartesian variables is used. Due to this transformation, centrifugal stiffening and gyroscopic coupling effects can be captured in linear potential and kinetic energy equations respectively. This makes the formulation less cumbersome compared to geometrically nonlinear modelling method. Moreover, this method provides the advantage of inclusion of gyroscopic coupling. The effect of gyroscopic coupling makes the structural model more realistic and the effects of gyroscopic coupling and centrifugal stiffening on the free vibration are highlighted in the Section 4.

From Eqs. 17-22 it can be observed that all the equations of governing system are coupled. $u_o - w_o$, $v_o - \phi$ and $\theta_x - \phi$ motions are coupled with gyroscopic terms. Depending on the composite ply angle lay up, many constants in the governing system vanishes resulting in decoupling. It can be observed that for a ply angle of $\theta = 0^\circ$ and $\theta = 90^\circ$, structural coupling between $u_o - v_o$, $u_o - \theta_x$ and $u_o - \phi$ vanishes. Consequently, governing system of equations decouples into two subsystems representing motions $u_o - w_o - \theta_y$ and $v_o - \theta_x - \phi$.

In the present study, extended Galerkin's method is used to obtain the approximate solution. In this approach discretization is carried out within the Hamilton's equation. The natural boundary conditions are taken back into the variational equation by carrying out reverse integration in space. Hence, only geometric boundary conditions appear as boundary terms. Thus consider $u_o = \varphi_1 q_1$, $v_o = \varphi_2 q_2$, $w_o = \varphi_3 q_3$, $\theta_x = \varphi_4 q_4$, $\theta_y = \varphi_5 q_5$ and $\phi = \varphi_6 q_6$ where, $\varphi_i(z)$ and $q_i(t)$ are vectors of trial function which satisfy geometric boundary conditions and generalized coordinates respectively. Upon substituting these quantities, the equations of motion can be written in the matrix form as,

$$M\ddot{q} + G_c\dot{q} + Kq = F_{CF} + R(t) + Fu(t) \tag{32}$$

where $F_{CF}\left(= \int_0^L 2b_1\Omega^2(R_o + z)\mathrm{d}z\right), R(t)$ and F are centrifugal force vector, arbitrary excited load and electric force vector respectively. Components of electric force vector are defined in Appendix C.

2.5 Sensor equation

Total charge generated on the sensor surface is the spatial summation of all the point charges on the sensor layer (Ray, 1998),

$$q_s(t) = \int_A D_1 H(s,z)\mathrm{d}A \tag{33}$$

Therefore, current on the surface of a sensor can be written as,

$$i(t) = \frac{\mathrm{d}q_s(t)}{\mathrm{d}t} = [C_s]\dot{q} \tag{34}$$

Components of C_s are defined in Appendix C.

2.6 Modal model

In formulating the reduced order model, it is assumed that the lower order modes have lower energy associated and consequently are the most easily excitable one. First r lower order modes are utilized as a transformation matrix between the generalized coordinates q and the modal coordinates η. Therefore,

$$q(t) = \sum_{i=1}^{r} \psi_i \eta_i \tag{35}$$

where ψ is the truncated eigen vector matrix. Eq. 32 can be written in reduced order form as,

$$\overline{M}\ddot{\eta}(t) + (\overline{G}_c + C_d)\dot{\eta}(t) + \overline{K}\eta(t) = \psi^{\mathrm{T}}F_{CF} + \psi^{\mathrm{T}}R(t) + \psi^{\mathrm{T}}Fu(t) \tag{36}$$

where $\overline{M} = \psi^{\mathrm{T}} M \psi$,$\overline{G}_c = \psi^{\mathrm{T}} \overline{G}_c \psi$ and $\overline{K} = \psi^{\mathrm{T}} K \psi$ are $r \times r$ reduced mass, gyroscopic and stiffness matrices respectively.$C_d = 2\xi_i \omega_i$ is the modal damping matrix and ξ_i is the modal damping ratio.

3 Optimal LQG control

In LQG controller, full state feedback LQR gain and the Kalman filter state estimation is done separately. Kalman filter is designed with the assumption of Gaussian distribution of white noise. State space form of Eq. 36 can be written as,

$$\dot{X}(t) = AX(t) + Bu(t) + W_f[F_{CF}(t) + R(t)] + w(t) \tag{37}$$

where $X = [\eta^{\mathrm{T}} \dot{\eta}^{\mathrm{T}}]$ is the state vector.

$$y(t) = CX(t) + v(t) \tag{38}$$

where $w(t)$ and $v(t)$ are Gaussian white noises and correlation matrices of these white noises can be expressed as, $E[w(t)w(t)^{\mathrm{T}}] = W$; $E[v(t)v(t)^{\mathrm{T}}] = V$. Matrices A, B, W_f and C can be written as,

$$A = \begin{bmatrix} 0 & I \\ -\overline{M}^{-1}\overline{K} & -\overline{M}^{-1}(C_d + \overline{G}_c) \end{bmatrix};$$

$$B = \begin{bmatrix} 0 \\ -\psi^{\mathrm{T}}\overline{M}^{-1}F \end{bmatrix};$$

$$W_f = \begin{bmatrix} 0 \\ \psi^{\mathrm{T}}\overline{M}^{-1} \end{bmatrix};$$

$$C = [0 \;\; C_s\psi]$$

The optimal control $u(t)$ is obtained from estimated state and measured output. Therefore, the actuator input voltage for the plant (Eq. 37) can be written as [Frank and Vassilis (1995)]

$$u(t) = -KX_e \tag{39}$$

where $K = R^{-1}B^{\mathrm{T}}P$ is the LQR gain and P is obtained by solving algebraic Reccati equation

$$PA + A^{\mathrm{T}}P + Q - PBR^{-1}B^{\mathrm{T}}P = 0 \tag{40}$$

X_e is the estimated state that is obtained by solving the differential equation,

$$\dot{X}_e = (A - BK - LC)X_e + Ly \tag{41}$$

where $L = SC^{\mathrm{T}}V^{-1}$ is the Kalman gain and S is obtained by solving filter Reccati equation

$$AS + SA + W - SC^{\mathrm{T}}V^{-1}CS = 0 \tag{42}$$

4 Results and discussions

To validate the present method, the results of present method are compared with the experimental and theoretical results of Ramesh and Inderjit (1992) for graphite epoxy beam are shown in Tab. 1. For validation, considered material properties are E_1 =141.93 GPa; E_2 =9.788 GPa; G_{12} =6.135 GPa; ρ =1444.8 kg/m^3, with beam geometric configuration (Fig. 1) $L = 0.84455$ m; $R_o = 0.06985$ m; $h = 0.762$ mm; $c = 11.4046$ mm; b =6.8834 mm; k =6 and $\theta = 30^\circ$. Based on the % deviation with the experimental results, it can be observed that present results are in good agreement with the experimental results. Furthermore, the results obtained by the present method are in close agreement with the theoretical results obtained by Ramesh and Inderjit (1992).

4.1 Numerical examples

The beam considered is of graphite-epoxy material with propertiesE_1 =206.8 GPa; E_2 =5.17 GPa; $G_{12} = G_{13}$ =3.1 GPa; G_{23} =2.5511 GPa; γ_{12} =0.25; ρ =1528.15 kg/m^3, with beam geometric configuration (Fig. 1) L =2.023 m; R_o =0.2023 m; h =10.16 mm; c =0.127 m; b =0.0254 m. The trial functions selected to satisfy geometric boundary conditions at the beam root ($z = 0$) are (φ_1, φ_2, φ_3, φ_4, φ_5, φ_6) = ($[z^2 z^3 \ldots]$, $[z^2 z^3 \ldots]$, $[zz^2 \ldots]$, $[zz^2 \ldots]$, $[zz^2 \ldots]$, $[z^2 z^3 \ldots]$).

Commercially available MFC properties are (www.smart-material.com) considered as, E_1 =30.4 GPa; E_2 =15.86 GPa; $G_{12} = G_{13}$ =5.52 GPa; γ_{12} =0.31; ρ =8528 kg/m^3; d_{11} =460 pC/N; d_{12} =-210 pC/N; A_p =(85×57) mm; h_p =0.3 mm.

The first three normalized eigen modes in lagging and flapping motions respectively, for a 30° ply angle are shown in Figs. 2 and 3. In both lagging and flapping modes, the beam gets straightened for rotating beam. It is because of centrifugal stiffening effect increases with rotational speed.

Table 1: Comparison of natural frequencies with experimental results

	Rotati-onal speed (rad/s)	Ramesh and Inderjit (1992)			
		Expt.	Theory	Present	%deviation with Expt. results
Flap I	0	21.1	19.8	19.84	5.97
	1000	28.3	26.8	26.15	7.59
Lag I	0	37.6	37.1	36.35	3.32
	1000	39.1	37.5	38.05	2.68
Flap II	0	127.8	124.2	129.6	1.39
	1000	134.9	131	138.17	2.37

In lagging motion (Figs. 2(a)-2(c)), the gyroscopic coupling (GC) effect straighten the beam more compared to the analysis neglecting GC. In flapping motion (Figs. 3(a)-3(c)), plot with and without GC are superimposed on one another. Thus, the GC does not play significant role in flapping motion. Hence the effect of GC between flapping and twisting motion can be neglected.

In Fig. 4, the first two coupled natural frequencies for various rotational speeds and taper parameters are illustrated. It is observed that a tapered beam yields higher natural frequencies than a uniform cross-section beam as shown in Figs. 4(a)-4(b). It is also shown that as the rotational speed increases, the natural frequency also increases causes the beam stiffened. Stiffening is more pronounced at higher rotational speeds because of combined effect of taper and centrifugal stiffening. It is also observed that as the rotational speed increases, the dominant motion changes from flap to lag and vice versa.

The first three gyroscopically coupled and uncoupled natural frequencies of coupled $u_o - w_o - \theta_y$ motion for various rotational speeds are shown in Fig.5. It is noticed that instability occurs for the considered beam configuration at rotational speed ≈ 1520 rad/s, which means the dominant first natural frequency, becomes zero. Hence rotational speed ≈ 1520 rad/s is the buckling speed. This result is well justified by Yoo and Shin (1998) who observed similar trends for metallic beams.

Figure 6 shows the effect of ply angle on forced vibration for a rotational speed 200 rad/s and modal damping ratio of 0.0005. It demonstrates that increase in the ply angle, tip displacement reduces. The maximum tip displacement reduces by 1.24%, 16.18% and 52.24% for the ply angles of 30°, 60° and 90° respectively, as compared to 0° ply angle beam. The system response can be altered by suitably selecting the ply angle, thus composite beam facilitates to control the response by structural tailoring.

The effect of number of modes considered in reduced order model is shown in Figs. 7(a) and 7(b). The beam considered in the present analysis is composed of 6 layers of anti-symmetric configuration with the ply angle of 30°. Two collocated actuator and sensor pairs located at 0 mm and 100 mm from the root of the beam are considered. Number of reduced order modes should be large enough, such that the effect of residual modes can be neglected. Here number of reduced order modes is selected by analyzing convergence of tip displacement and actuator voltage. It is found that first five low frequency modes are sufficient for the convergence of tip displacement (Fig. 7(a)) and actuator voltage (Fig. 7(b)). Hence further analysis is carried out by considering five low frequency modes in the reduced order model.

The bending vibration controlled response for a rectangular pulse and rotational speed of 200 rad/s are shown in Fig. 8(a). Co-located four actuators and sensors are considered as equally distributed between 0 - 70% span of beam. Actuators are numbered 1 to 4 starting from the root. Voltages applied on each actuator are presented in Fig. 8(b). It clearly shows that maximum tip displacement and control voltages applied on all four actuators for 60° ply angle is less as compared to 30° ply angle. Also, settling time for 60° ply angle beam is less compared with 30° ply angle beam.

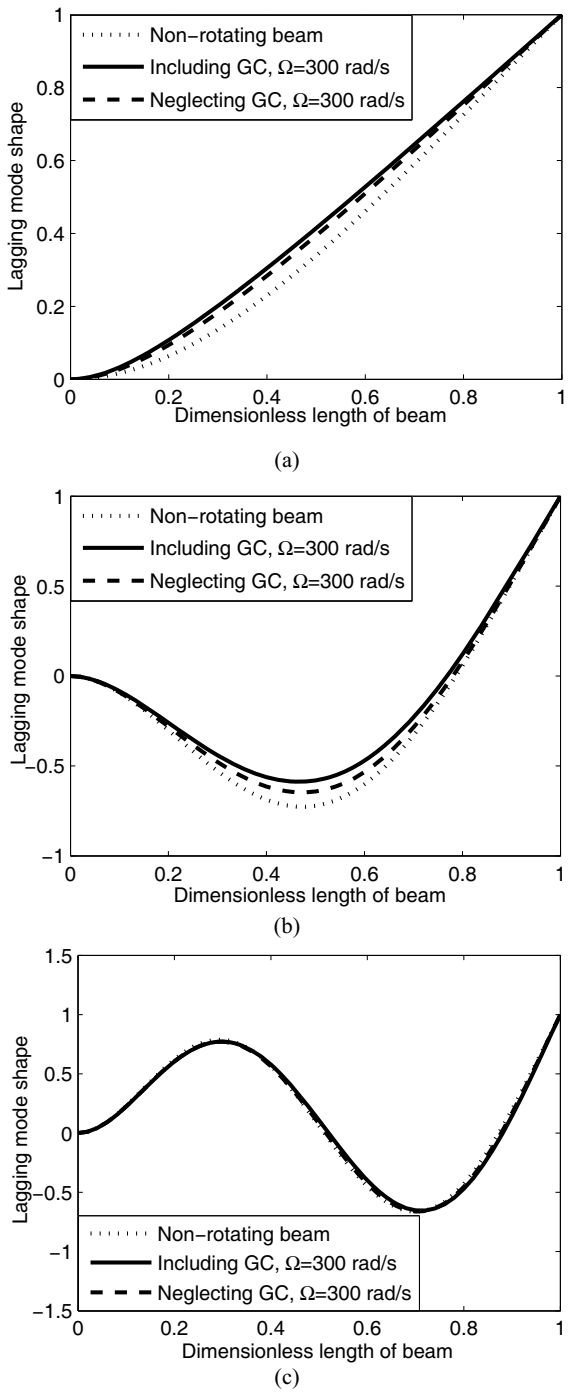

Figure 2: First three normalized lagging mode shape variation (a) first mode (b) second mode (c) third mode

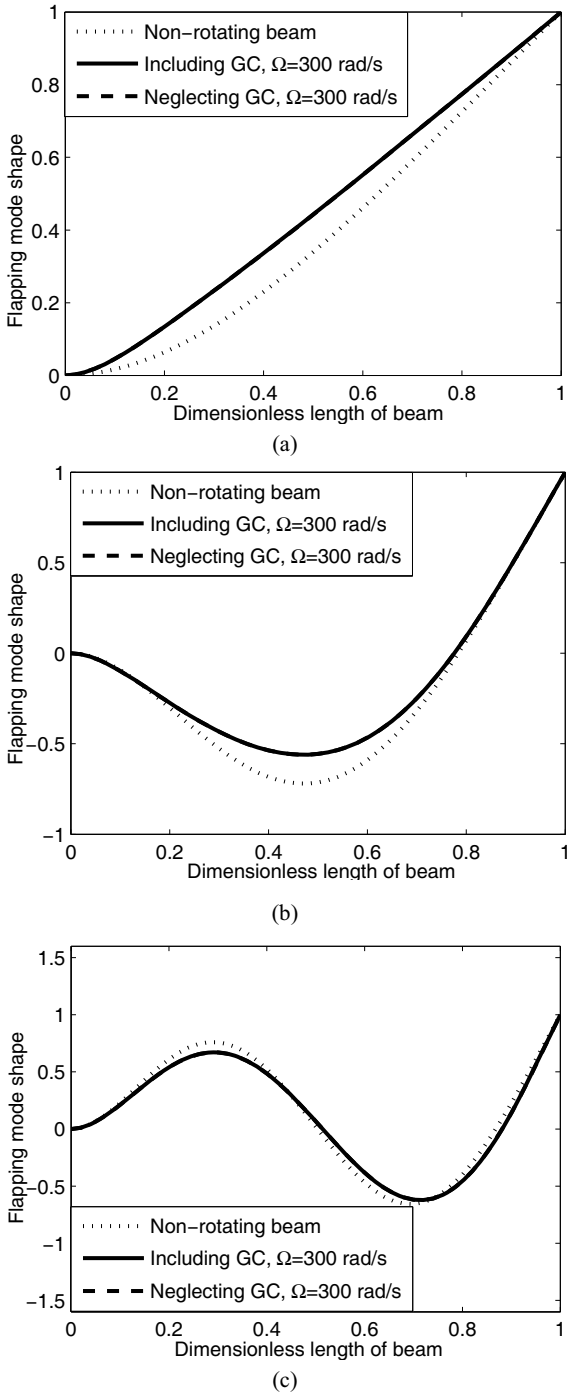

Figure 3: First three normalized flapping mode shape variation (a) first mode (b) second mode (c) third mode

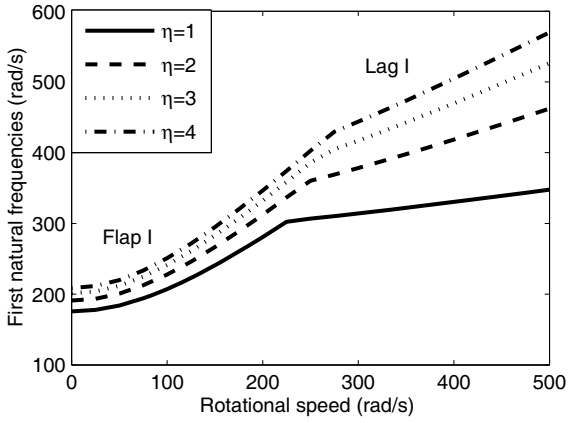

(a)

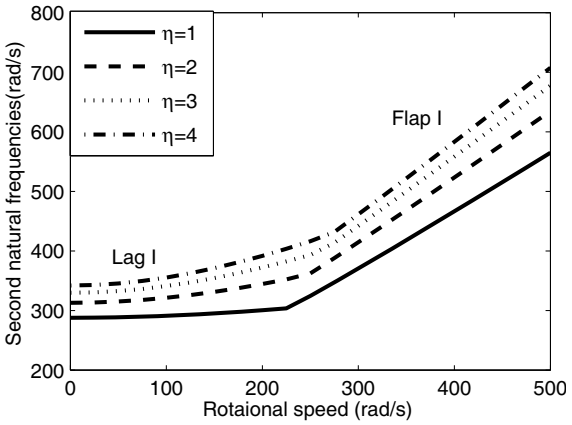

(b)

Figure 4: First two coupled natural frequencies with rotational speeds for various taper parameters (η). (a) first natural frequencies (b) second natural frequencies

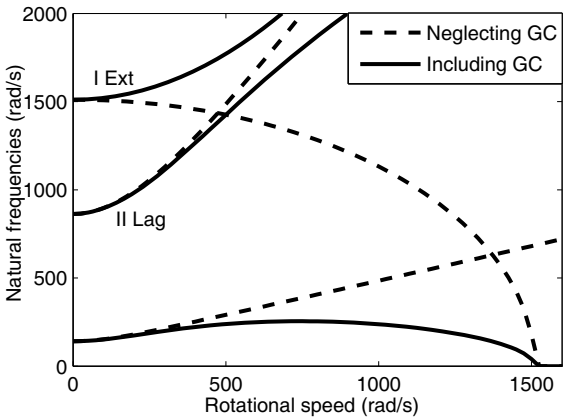

Figure 5: Variation of first three coupled lagging-extension natural frequencies with rotational speeds for a 0° ply angle

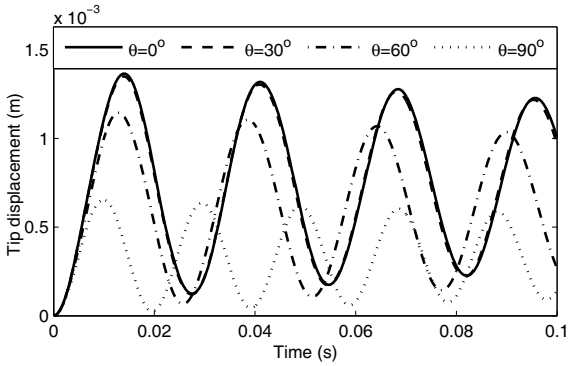

Figure 6: Effect of ply angle on forced vibration for step forcing

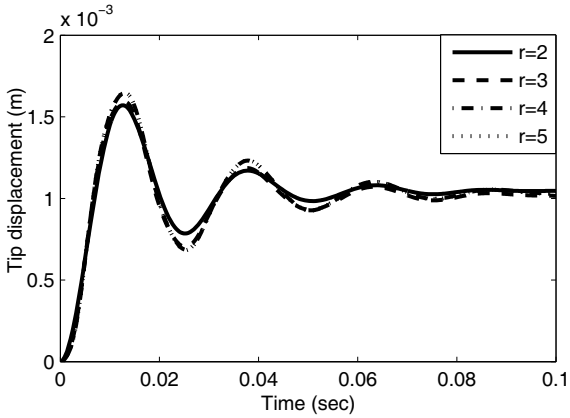

(a)

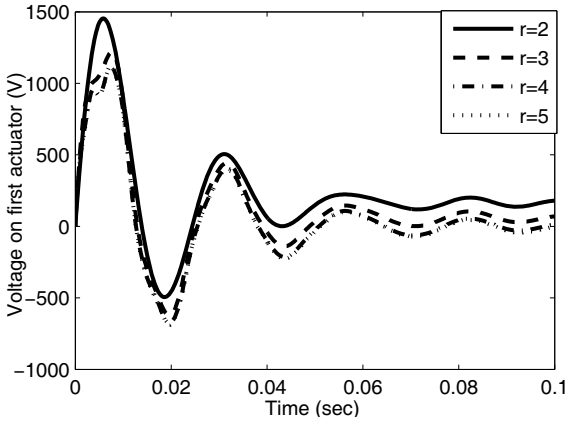

(b)

Figure 7: Effect of number of modes considered in reduced order model for rectangular forcing (a) tip displacement (b) applied voltage on first actuator

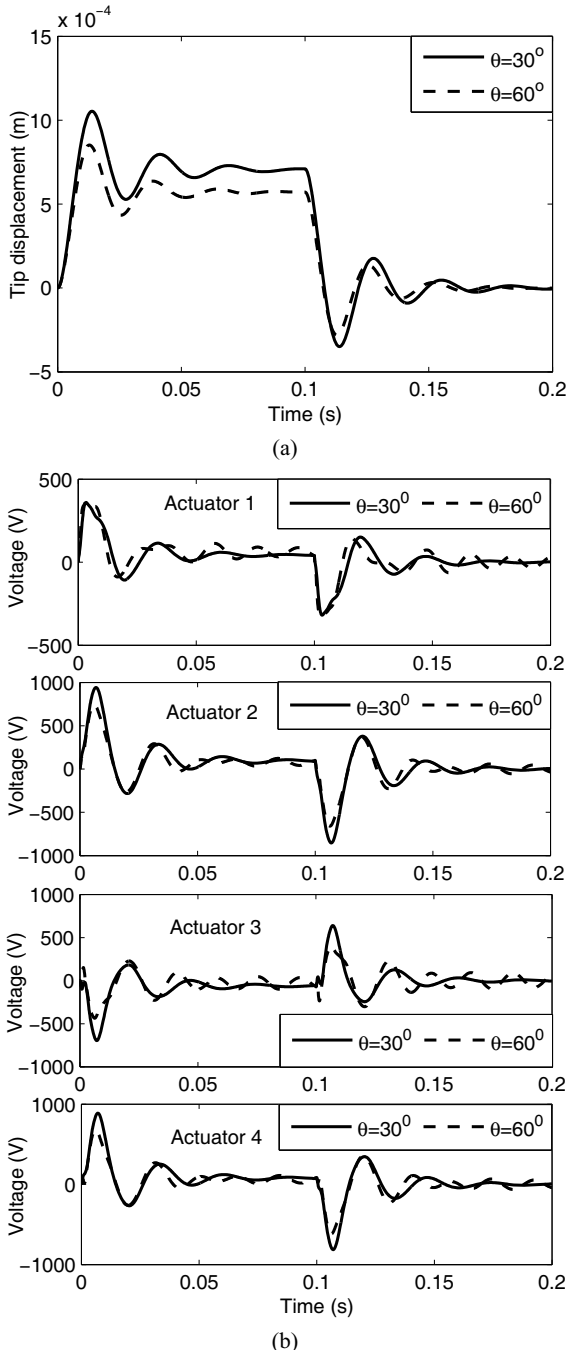

Figure 8: Effect of ply angle for a rectangular forcing and rotational speed of 200 rad/s (a) tip displacement (b) actuator voltage

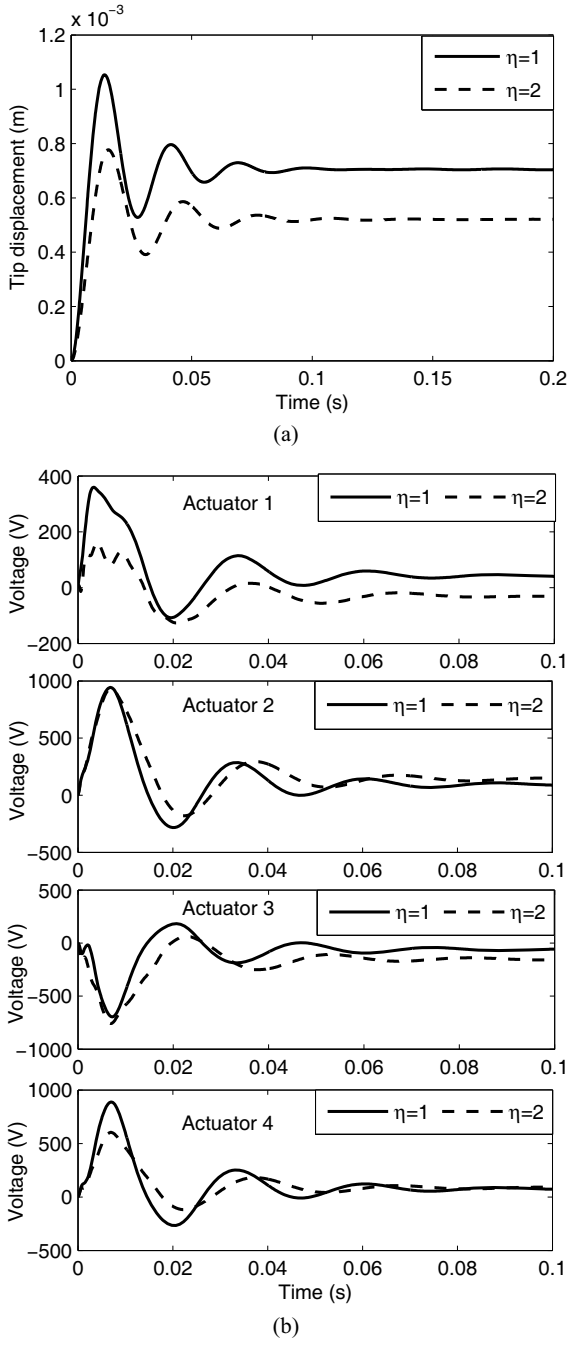

Figure 9: Effect of taper parameter for a rectangular forcing and rotational speed of 200 rad/s (a) tip displacement (b) actuator voltage

The effect of taper parameter on tip displacement and control voltage for a step forcing and rotational speed of 200 rad/s are presented in Figs. 9(a) and 9(b) respectively. It is observed increase in taper, decreases the maximum tip displacement and maximum voltage applied on the 1^{st}, 3^{rd} and 4^{th} actuators. But, increase in taper, marginally increases applied voltage on the 2^{nd} actuator. For the present configuration, voltages applied on the actuator are well below the upper limit of the MFC actuator of 1500V.

5 Conclusions

In this work, structural modelling of rotating beam including effect of embedded MFC sensors and actuators using HSDT model has been presented. Equations of motion have been derived using hybrid deformation variables, which employ stretch deformation instead of the conventional axial deformation. Coupled analysis is performed and the effect of gyroscopic coupling on natural frequencies presented in numerical example. Control problem has been solved by LQG algorithm. Optimal performance of MFC actuators and sensors for vibration suppression of rotating composite beams has been studied. Results reveal that,

- GC between lagging-extension is having considerable effect on the system natural frequency and mode shape and hence cannot be neglected.
- Taper in beam enhances the first two natural frequencies of the system.
- System response can be altered by changing the ply angle orientation.
- MFC sensors and actuators can be used for vibration sensing and feedback control of rotating composite beams.
- Tip displacement and control voltage can be reduced by increasing the fiber orientation.

Mathematical model is derived for arbitrary configuration, which can be easily extended to other configurations like elliptical cross-section and airfoil cross-section beam in further studies. Structural model can be extended to include the effect of pretwist and presetting as well. Optimal placement of actuators and sensors is still a field of further research.

References

Bent, A. A.; Hagood, N. W.; Rodgers, J. P. (1995): Anisotropic actuation with piezoelectric fiber composites. *J Intelligent Material Systems and Structures*, vol. 6, no. 3, pp. 338-349.

Brockmann, T. H.; Lammering, R. (2006): Beam finite elements for rotating piezoelectric fiber composite structures. *J Intelligent Material Systems and Structures*, vol. 17, pp.431-447.

Chandiramani, N. K.; Librescu, L; Shete, C. D. (2002): On the free vibration of rotating composite beams using a higher order shear formulation. *Aerospace Science and Technology*, vol. 6, pp. 545-561.

Chandiramani, N. K.; Librescu, L. I.; Saxena, V.; Kumar, A. (2004): Optimal vibration control of a rotating composite beam with distributed piezoelectric sensing and actuation. *Smart Materials and Structures,* vol. 13, pp. 1-10.

Choi, S. C.; Park, J. S; Kim, J. H. (2006): Active damping of rotating composite thin walled beams using MFC actuators and PVDF sensors. *Composite Structures*, vol. 76, pp. 362-374.

Choi, S. C.; Park, J. S; Kim, J. H. (2007): Vibration control of pretwisted rotating composite thin walled beams with piezoelectric fiber composites. *J Sound and Vibration*, vol. 300, pp. 176-196.

Frank, L. L.; Vassilis, L. S. (1995): Optimal control. John Wiley & Sons, Inc., Second Edition, pp. 459-478.

Henry, A. S.; Gyuhae, P.; Daniel, J. I. (2004): An investigation into the performance of macro fiber composites for sensing and structural vibration applications. *Mechanical Systems and Signal Processing*, vol. 18, pp. 683-697.

Kane, T. R.; Ryan, R. R.; Banerjee, A. K. (1987): Dynamics of beams attached to a moving

base. *J Guidance, Control, and Dynamics*, vol. 10, no.2, pp. 139-151.

Lam, Y. K.; Peng, X. Q.; Liu, R. G.; Reddy, J. N. (1997): A finite element model for piezoelectric composite laminates. *Smart Materials and structures*, vol. 6, pp. 583-591.

Mitra, M.; Gopalakrishnan, S.; Bhat, M. S. (2004a): A new super convergent thin walled composite beam element for analysis of box beam structures. *Int. J. of Solids and Structures*, vol. 41, no. 5-6, pp. 1491-1518.

Mitra, M.; Gopalakrishnan, S.; Bhat, M. S. (2004b): Vibration control in a composite box beam with piezoelectric actuators. *Smart Materials and structures,* vol. 13, no. 4, pp. 676-690.

Narayanan, S; Balamurugan, V. (2003): Finite element modelling of piezolaminated smart structures for active vibration control with distributed sensors and actuators. *J Sound and Vibration*, vol. 262, pp. 529-562.

Nilanjan, M.; Ray, M. C. (2004): Exact solutions for the analysis of piezoelectric fiber reinforced composites as distributed actuators for smart composite plates. *International J Mechanics and Materials in Design*, vol. 1, pp. 347-364.

Park, J. E.; Kim, J. H. (2005): Analytical development of single crystal macro fiber composites actuators for active twist rotor baldes. *Smart Materials and Structures*, vol. 14, pp. 745-753.

Ramesh, C.; Inderjit, C. (1992): Experimental theoretical investigation of the vibration characteristics of rotating composite box beams. *J Aircraft*, vol. 29, no. 4, pp. 657-664.

Ray, M. C. (1998): Optimal control of laminated plate with piezoelectric sensor and actuator layers. *AIAA Journal*, vol. 36, no. 12, pp. 2204-2208.

Reddy, J. N. (1999): On laminated composite plates with integrated sensors and actuators. *Engineering Structures*, vol. 21, pp. 568-593

Song, O; Librescu, L. (1997): Structural modeling and free vibration analysis of rotating composite thin-walled beams. *J the American Helicopter Society*, vol. 42, no. 4, pp. 358-369.

Sungsoo, N.; Liviu, L. (2000): Optimal vibration control of thin walled anisotropic cantilevers exposed to blast loadings. *J Guidance, Control, and Dynamics*, vol. 23, no. 3, pp. 491-499.

Suresh, J. K.; Nagaraj, V. T. (1996): Higher order shear deformation theory for thin walled composite beams. *J Aircraft*, vol. 33, no. 5, pp. 978-986.

Vasques, C. M. A.; Rodrigues, J. D. (2006): Active vibration control of smart piezoelectric beams: comparison of classical and optimal feedback control strategies. *Computers and Structures*, vol. 84, pp. 1402-1414.

Vinod, K. G.; Gopalakrishnan, S.; Ganguli, R. (2006): Wave propagation characteristics of rotating uniform Euler-Bernoulli beams. *CMES: Computer Modeling in Eng. and Sci.*, vol.16, no.3, pp. 197-208.

Vinod, K. G.; Gopalakrishnan, S.; Ganguli, R. (2007): Free vibration and wave propagation analysis of uniform and tapered rotating beams using spectrally formulated finite elements. *Int. J. of Solids and Structures*, vol. 44, no. 18-19, pp. 5875-5893.

Wilkie, W. K.; Belvin, W. K.; Park, K. C. (1996): Aeroelastic analysis of helicopter rotor blades incorporating anisotropic piezoelectric twist actuation. *Proceedings of ASME 1996 World Congress and Exposition, Adaptive Structures Symposium*, November.

Yoo, H. H.; Lee, S. H.; Shin, S. H. (2005): Flapwise bending vibration analysis of rotating multilayered composite beams. *J Sound and Vibration*, vol. 286, no. 4-5, pp. 745-761.

Yoo, H. H.; Rayn, R. R.; Scott, R. A. (1995): Dynamics of flexible beams undergoing overall motions. *J Sound and Vibration*, vol. 181, no. 2, pp. 261-278.

Yoo, H. H.; Shin, S. H. (1998): Vibration analysis of rotating cantilever beams. *J Sound and Vibration*, vol. 212, no. 5, pp. 807-828.

Website MFC material properties, at http://www.smart-material.com/Smart-choice.php?from=MFC

Appendix A: Linear strain displacement relations

$$\varepsilon_{xx} = u_{,x};\ \ \varepsilon_{yy} = v_{,y};\ \ \varepsilon_{zz} = \hat{s}_{,z};\ \ \gamma_{xy} = \tfrac{1}{2}(u_{,y} + v_{,x});$$

Appendix B: Global stiffness quantities of piezoelectric material

$$\tilde{a}_1^p = \oint P_1 \mathrm{d}s;$$
$$\tilde{a}_3^p = \oint \left[\frac{4P_6}{h^2} - P_4\right] m^p \mathrm{d}s$$
$$\tilde{a}_3^p = \oint \left[-\frac{4P_3}{h^2} - P_2\right] m^p \mathrm{d}s;$$
$$\tilde{a}_6^p = \oint \left[\frac{4P_2 m^p}{h^2} + P_1 \overline{y}^p\right] \mathrm{d}s;$$
$$\tilde{a}_9^p = \oint \left[-\frac{4P_6}{h^2} + P_4\right] m^p \mathrm{d}s;$$
$$\tilde{a}_{10}^p = \oint \left[4P_4\psi + 2P_5\right] \mathrm{d}s;$$

where, local piezoelectric constants are obtained as,

$$P_1 = \frac{L_{11}A_{12}}{A_{11}} - L_{12}; \quad P_2 = \frac{L_{11}B_{12}}{A_{11}} - M_{12};$$
$$P_3 = \frac{L_{11}D_{12}}{A_{11}} - O_{12}; \quad P_4 = \frac{L_{11}F_{12}}{A_{11}} - L_{12};$$
$$P_5 = \frac{L_{11}A_{16}}{A_{11}}; \qquad P_6 = \frac{L_{11}B_{16}}{A_{11}};$$
$$P_7 = \frac{L_{11}D_{12}}{A_{11}};$$

Stiffness and piezo coefficients are,

$$(A_{ij}, B_{ij}, D_{ij}, F_{ij}, H_{ij}, I_{ij}, J_{ij})$$
$$= \int_{-h/2}^{h/2} \overline{Q}_{ij} \left(1, n, n^2, n^3, n^4, n^5, n^6\right) \mathrm{d}n;$$
$$(L_{ij}, M_{ij}, O_{ij}, R_{ij}) = \int_{h/2-t_P}^{h/2} \overline{e}_{ij} \left(1, n, n^2, n^3\right) \mathrm{d}n;$$

Appendix C: Components of F and C_s

$$F_1 = \frac{\tilde{a}_3^p \phi_1'}{h_p}; \quad F_2 = \frac{\tilde{a}_4^p \phi_2''}{h_p}; \quad F_3 = \frac{\tilde{a}_1^p \phi_3'}{h_p};$$
$$F_4 = \frac{\tilde{a}_6^p \phi_4'}{h_p}; \quad F_5 = \frac{\tilde{a}_9^p \phi_5}{h_p}; \quad F_6 = \frac{\tilde{a}_6^p \phi_6'}{h_p};$$

$$C_1 = \frac{h}{6} m^p \phi_1''; \quad C_2 = \frac{h}{6} m^p \phi_2''; \quad C_3 = \phi_3';$$
$$C_4 = \frac{h}{6} m^p \phi_4'; \quad C_5 = \frac{h}{6} m^p \phi_5'; \quad C_6 = ha\phi_6'';$$